Maximal charge injection of consecutive electron pulses with uniform temporal pulse separation

Y. L. Liu,[1,2] P. Zhang,[3] S. H. Chen,[1] and L. K. Ang[2,a)]
[1]Department of Physics, National Central University, Jhongli 32001, Taiwan
[2]Engineering Product Development, Singapore University of Technology and Design, Singapore 487372
[3]Department of Nuclear Engineering and Radiological Sciences, University of Michigan, Ann Arbor, Michigan 48109-2104, USA

(Received 16 February 2015; accepted 30 July 2015; published online 13 August 2015)

A charge sheet model is proposed for the study of the space-charge limited density of consecutive electron pulses injected to in a diode with uniform temporal pulse separation. Based on the model, an analytical formula is derived for expressing the dependency of the charge density limit on the gap spacing, gap voltage, and pulse separation. The theoretical results are verified by numerical solutions up to electron energy of a few MeV, including relativistic effects. The model can be applied to the design of multiple-pulse electron beams for time resolved electron microscopy and free electron lasers. © *2015 AIP Publishing LLC*. [http://dx.doi.org/10.1063/1.4928586]

Photoemission electron microscopy (PEEM, also known as photoelectron microscopy, PEM) generates electron pulses by using photocathodes and records the information of the interaction between the electrons and the sample for imaging purposes. Brüche first reported on the use of PEEM with ultra-violet (UV) radiation to excite electron photoemission in 1933.[1] These developments led to many modern electron microscopic techniques, such as time resolved PEEM (TR-PEEM), which is well suited for the real-time observation of fast processes on surfaces equipped with pulsed synchrotron radiation for illumination,[2] time-of-flight PEEM (TOF-PEEM), which is PEEM using an ultrafast gated CCD camera or a time-and space-resolving counting detector for observing fast processes on surfaces,[3] multiphoton PEEM (Multiphoton PEEM), which is employed for the study of localized surface plasmon excitations in nanoclusters or for direct spatial observation of the hot-electron lifetime in structured films using femtosecond lasers,[4] and ultra-fast electron microscopy (UEM), which is used to study structural dynamics with space- and time-resolutions that allow direct observation of transformations affecting the fundamental properties of materials using timed-pulse electron imaging and selected-area diffraction.[5] For a brief review paper, introducing the history of PEEM please see Ref. 6. Dependent on the current density and pulse duration of the electron pulses, the space charge effect may play an important role in electron gun design and the performance of electron microscopy.

At the high current regime, it is known that the space charge effect will limit the maximum injected current density. Consider a one-dimensional (1D) planar diode with gap distance d and gap voltage V_g. The maximal steady-state space-charge-limited current (SCLC) density is given by the classical Child-Langmuir (CL) law[7,8]

$$J_{CL} = \frac{4}{9}\epsilon_0\sqrt{\frac{2e}{m}}\frac{V_g^{\frac{3}{2}}}{d^2}, \quad (1)$$

where e and m are, respectively, the charge and mass of the electron, and ϵ_0 is the free space permittivity. In the past 50 years, the CL law has been revised extensively to consider various effects such as finite emission area,[9–11] short pulse length,[12–14] relativistic (and quantum) effects,[13–15] as well as semi-analytical scaling for cylindrical and spherical diodes,[16] and drift space setting.[17–20]

Taking UEM as an example for application in this paper, we first briefly introduce the background. The UEM methodology is based upon the stroboscopic pump-probe technique,[21] which is used to make a cyclically moving object appear to be slow-moving, or stationary. The main difference between UEM and the spectroscopic pump-probe techniques[22] is that electrons, rather than photons, are used to probe the sample. The use of electrons as probes allows for analysis of the actual atomic-scale structural changes induced by the pump laser pulse, because of the much shorter wavelength of fast electrons from the de Broglie relation. By using well-separated short electron multi-pulses, UEM enables the observation not only of three-dimensional (3D) spatial information but also temporal information.[23–27] Hence, UEM is a four-dimensional (4D) electron microscopy that is important for many applications in physics, chemistry, biology, and materials sciences. To have good spatial resolution, one would like to have a sufficient charge per pulse. However, a higher charge will cause distortion of the time interval between the pulses and also pulse broadening that may affect the time resolution. As reported in Ref. 28, space charge effects can broaden the electron pulse to many times its original length and generate many eV of kinetic energy bandwidth in only a few nanoseconds. In a typical single-pulse UEM operation with a gap voltage $V_g = 120\,\text{kV}$, gap spacing $d = 25\,\text{mm}$, and spot size diameter of $30\,\mu\text{m}$, the electron number is equal to 1.88×10^5,[28] which is about 3 [nC/cm^2]. It is thus shown that space charge effects between the pulses will be important if operated in multi-pulse mode.

In this paper, we are interested in following along this line of study by creating a charge sheet model to derive an

a)Electronic mail: ricky_ang@sutd.edu.sg

analytical or semi-analytical formula that is able to predict the maximum amount of charge density per pulse for a train of N pulses allowed by the space charge effects without distorting the pulse interval. The results should enable one to know the upper limit of the charge density per pulse for any desirable pulse interval, gap spacing, and applied voltage in a diode. It has been shown recently that the space charge effects can be suppressed by having the electron beam in the relativistic regime (3–5 MeV) in single shot transmission electron microscopy (TEM).[29] In this study, we will also show that our model is applicable for electron beam energies of up to a few MV including relativistic effects.

Consider a single charge sheet of charge density σ propagating in a diode with zero initial velocity, as shown in Fig. 1(a). By solving the Poisson's equation $\varphi'' = -\frac{\sigma}{\epsilon_0}\delta(x - x_1)$, the electric field profiles are $E_1 = -\frac{V_g}{d} + \frac{\sigma}{\epsilon_0}\left(\frac{x_1}{d}\right)$, $E_2 = -\frac{V_g}{d} - \frac{\sigma}{\epsilon_0}\left(1 - \frac{x_1}{d}\right)$, and $E_{b1} = \frac{1}{2}[E_1 + E_2] = -\frac{V_g}{d} - \frac{\sigma}{\epsilon_0}\left[\frac{1}{2} - \frac{x_1}{d}\right]$, where E_1, E_2, and E_{b1} are the fields on the anode, the cathode, and the charge sheet, respectively.[18] If the charge sheet to be accelerated is located at the cathode ($x_1 = 0$), the equations become $E_1 = -\frac{V_g}{d}$, $E_2 = -\frac{V_g}{d} - \frac{\sigma}{\epsilon_0}$, and $E_{b1} = -\frac{V_g}{d} - \frac{\sigma}{2\epsilon_0}$. If we have zero electric field at the sheet ($E_{b1} = 0$), we have $\sigma_1 = -2\epsilon_0\frac{V_g}{d}$, and the charge sheet will not be accelerated due to the Coulomb blockade effect.[16,30] Note that the Coulomb blockade will be important at very high charge density, which is larger than σ_N [see Eq. (3) below]. In this paper, we will ignore this effect as the focus is on the $\sigma < \sigma_N$ regime.

To obtain the SCLC density, the condition is to have a zero electric field on the cathode ($E_2 = 0$), which gives $\sigma_1 = -\epsilon_0\frac{V_g}{d}$, and the SCLC density is given by $J_1 = \frac{\sigma_1}{\tau_p}$,

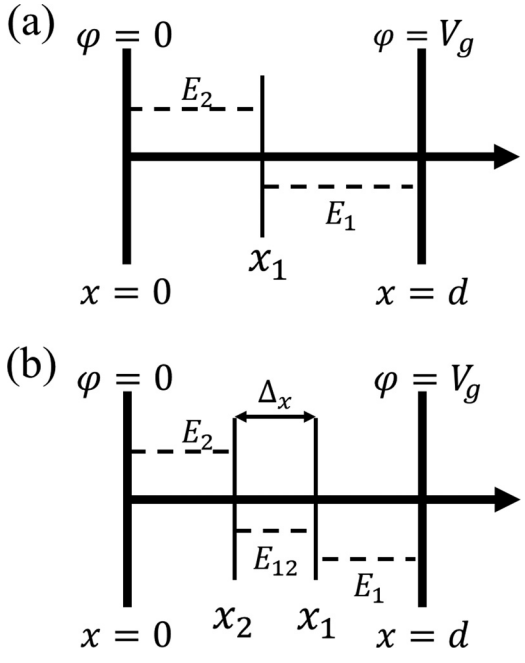

FIG. 1. An accelerating diode with gap spacing d and gap voltage V_g with (a) single beam injection and (b) N = 2 beam injections, respectively.

where τ_p is the pulse duration. A normalized time scale, $X_{CL} \equiv \frac{\tau_p}{T_{CL}}$, is introduced to define the ratio between the pulse duration and the transit time T_{CL} as in the CL law. The latter is expressed as $T_{CL} = \frac{3d}{\sqrt{2eV_g/m}}$ in the classical regime and $T_{RCL} = \frac{2d}{c}\frac{\left(\gamma_0^2 - 1\right)^{1/4}}{G(\gamma_0)}$ in the relativistic regime.[12,17] Here, $\gamma_0 = 1 + \frac{eV_g}{mc^2}$ is the Lorentz factor and $G(\gamma_0) = \int_1^{\gamma_0}(r^2 - 1)^{-1/4}dr$.

By solving $\varphi'' = -\frac{\sigma}{\epsilon_0}\sum_{n=1}^{N}\delta(x - x_n)$ for N number of pulses, the electric field on the cathode is

$$E_N = -\frac{V_g}{d} - \frac{\sigma}{\epsilon_0}\left(N - \sum_{n=1}^{N}\frac{x_n}{d}\right). \tag{2}$$

Since the pulse intervals are assumed to be uniform, as given by $\Delta_x = x_{n-1} - x_n$, the SCL charge density is

$$\sigma_N = \frac{\sigma_1}{N}\frac{1}{1 - \frac{\Delta_x}{d}\left(\frac{N-1}{2}\right)} = \frac{\sigma_1}{N}\frac{1}{1 - \frac{1}{2}\left(\frac{qE_0}{m}\right)\frac{\Delta_t^2}{d}\left(\frac{N-1}{2}\right)}, \tag{3}$$

where $\Delta_x \cong \frac{1}{2}\left(\frac{qE_0}{m}\right)\Delta_t^2$ due to the acceleration of pulses by the applied electric field $E_0 = -\frac{V_g}{d}$, and Δ_t is the time step of the beam injection (or the injection period). The dominant term in Eq. (3) is $\sigma_N \cong \frac{\sigma_1}{N}$, which would provide a very good approximation for small Δt. It is important to note that uniform temporal separation does not imply uniform spacing because of the external accelerating field E_0. Here, $\Delta x = \frac{1}{2}\left(\frac{qE_0}{m}\right)\Delta_t^2$ is a dimensional or normalized scale to give a rough estimation of the SCL charge density as shown in Eq. (3), which can be later tuned by introducing a factor $f = \sigma/\sigma_N$, where f is determined by finding the numerical solution for σ. The maximum number of charge sheets in the diode can be estimated by $N_{max} \cong \left\lceil\frac{T_0}{\Delta_t}\right\rceil$, where $T_0 \cong \sqrt{2d/\left(\frac{qE_0}{m}\right)}$ is the transit time of single charge sheet. For easy illustration, a diagram of the injection of two charge sheets is shown in Fig. 1(b).

To include the interaction between the sheets,[15,23] we solve the equation of motion (EOM) numerically for the position of each sheet x_n(t) that is injected into the diode. The normalized charge density (in terms of σ_1) is

$$\bar{\sigma}(\bar{t}) = 1 + \frac{\sigma_N}{\sigma_1}\sum_{n=1}^{N}\bar{x}_n(\bar{t}), \tag{4}$$

where $\bar{t} = \frac{t}{T_{CL}}$ and $\bar{x}_n = \frac{x_n(t)}{d}$ are the normalized time and position of the nth sheet, respectively. The normalized electric field (in terms of the applied field E_0) acting on each charge sheet is

$$\bar{E}_n(\bar{t}) = 1 + \frac{\sigma_N}{\sigma_1}\sum_{n=1}^{N}\bar{x}_n(\bar{t}) - \frac{\sigma_N}{\sigma_1}\left(n - \frac{1}{2}\right). \tag{5}$$

The normalized EOM given by

$$\begin{cases} \dfrac{d\bar{v}_n}{d\bar{t}} = 1.5\bar{E}_n(\bar{t}) \\ \dfrac{d\bar{x}_n}{d\bar{t}} = 3\bar{v}_n(\bar{t}) \end{cases} \tag{6}$$

are to be solved numerically with the initial conditions: $\bar{x}_n(0) = 0; \bar{v}_n(0) = 0$, where $\bar{v}_n = v_n/\sqrt{\frac{2eV_g}{m}}$. By using $J(t) = \frac{d\sigma(t)}{dt}$, we obtain the normalized current density (in terms of $\frac{\sigma_1}{T_{CL}}$) as

$$\bar{J}(\bar{t}) = 3\left(\frac{\sigma_N}{\sigma_1}\right)\sum_{n=1}^{N}\bar{v}_n(\bar{t}). \tag{7}$$

Unless otherwise mentioned, the following parameters, based on prior studies of ultrafast electron optics,[24] have been used in our calculation: $d = 1.5$ mm and $V_g = 30$ kV.[31] The corresponding transit time for a single charge sheet is $T_0 \cong \sqrt{\frac{2d}{eE_0/m}} \cong 29.2$ ps. We first consider the time step of the injection as $\Delta_t = 1$ ps. There are about $N_{max} \cong \frac{T_0}{\Delta_t} = 30$ charge sheets in a diode at steady state. Figs. 2(a) and 2(c), respectively, show the trajectories of each charge sheet and the current density, from the solution of Eq. (6) with a given

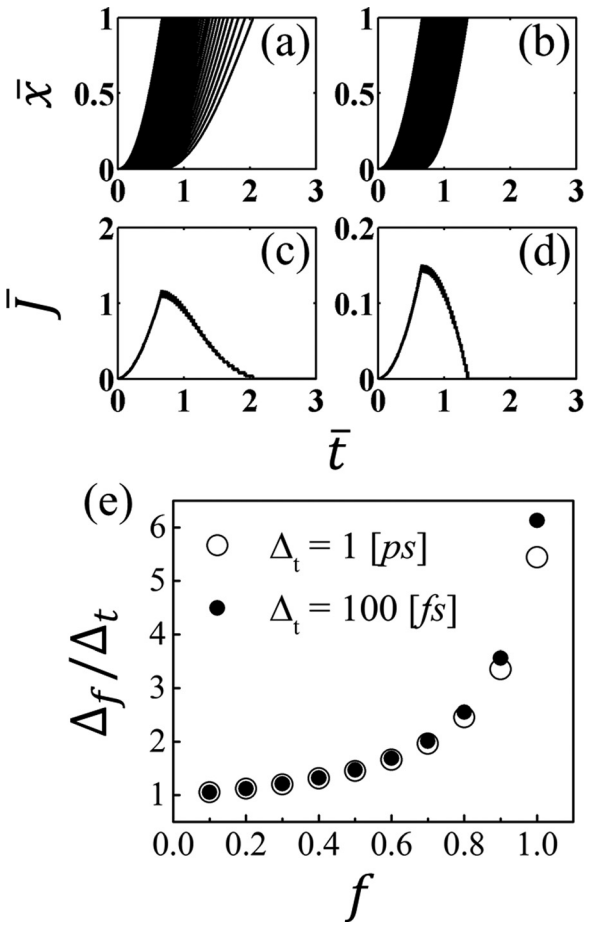

FIG. 2. The trajectories of each beam [(a) and (b)] and current densities [(c) and (d)] in a diode with gap spacing $d = 1.5$ mm and gap voltage $V_g = 30$ kV for $N = 30$ and $\Delta_t = 1$ps at $\sigma = \sigma_{N=30}$ [(a) and (c)] and $\sigma = 0.1\sigma_{N=30}$ [(b) and (d)]. (e) The dependence of Δ_f as a function of f for $\Delta_t = 1$ ps and $\Delta_t = 100$ fs.

charge density $\sigma = \sigma_{30}$ obtained from Eq. (3). It is found that the time interval between two adjacent charge sheets at the anode increases with time and the corresponding interval for the current density fluctuation is also extended, which is due to the space charge effect.

By defining Δ_f to be the final time interval for the last two charge sheets reaching at the anode, we can use Δ_f to measure the distortion of the pulse intervals. Here, we define f *as* $f = \sigma/\sigma_N$, where σ_N is a normalized scale factor as shown in Eq. (3). In the case of $f = 1$, we have $\Delta_f = 5.443$ ps, which is five times larger than the initial injection time step $\Delta_t = 1$ ps. It is clear that we need to reduce the injected charge density from $\sigma = \sigma_{30}$ to have $\Delta_f = \Delta_t$. Figures 2(b) and 2(d) show the corresponding results at $\sigma = 0.1\sigma_{30}$, and we have $\Delta_f = 1.054$ ps, which is only 5.4% higher than Δ_t.

Ultrafast time imaging requires a time resolution of less than 1 ps.[5] Here, we reduce the injection time step to $\Delta_t = 100$ fs, which gives $N_{max} \cong \lceil \frac{T_0}{\Delta_t} \rceil = 293$. Using the same calculation at $\sigma = \sigma_{293}$, we have $\Delta_f = 613$ fs, which is also about six times larger than Δ_t. Reducing the density to $\sigma = 0.1\sigma_{293}$, Δ_f is reduced to $\Delta_f = 105$ fs, which is about 5% higher than Δ_t. This finding indicates that Eq. (3) is a useful formula over a wide range of parameters, and 10% of its determined value seems to be able to ensure good uniform time intervals between the pulses. Figure 2(e) shows Δ_f as a function of f for the above two cases. The results clearly show that both cases converge to $\Delta_f \rightarrow \Delta_t$ for $f \rightarrow 0.1$.

At $f = 1$ or $\sigma = \sigma_N$, the electron trajectories show an unstable state, where the injected electron pulse may start being reflected back to the cathode if a large number of pulses are injected. Figures 3(a) and 3(c) show the trajectories and current densities after 60 charge sheet injections with $\Delta_t = 1$ps and $\sigma = 0.6\sigma_{30}$. Here, the maximal number of pulses allowed without reflection is $N = 30$. However, reflection may occur at lower charge densities than σ_{30} [from Eq. (3)]. In this case, reflection starts occurring at $\sigma = 0.6\sigma_{30}$ for $N = 60$. When a lower charge density of $\sigma = 0.1\sigma_{30}$ is considered with the same $N = 60$, stable trajectories and a flat current density were observed, as shown in Figs. 3(b) and 3(d). As shown in Fig. 3(e), we see the same convergence of $\Delta_f \rightarrow \Delta_t$ for $f \rightarrow 0.1$ over a wide range of $N = 120$, 60, 30, and 15. The bottom part of Fig. 3(e) shows the accuracy near $f \backsimeq 0$ to be 0.1, which shows that Δ_f is less than 10% higher than Δ_t at $f \leq 0.1$.

The classical model presented above can be extended to include relativistic effects when the applied voltage is comparable or larger than 511 kV, as in the case of the recent TEM performed at 5 MV.[29] In the relativistic regime, Eq. (6) becomes

$$\begin{cases} \dfrac{d\bar{u}_n}{d\bar{t}} = 2(\gamma_0 - 1)\dfrac{(\gamma_0^2 - 1)^{1/4}}{G(\gamma_0)}\left[1 + \bar{E}_n\sum_{n=1}^{N}\bar{x}_n(\bar{t}) - \bar{E}_n\left(n - \dfrac{1}{2}\right)\right] \\ \dfrac{d\bar{x}_n}{d\bar{t}} = 2\dfrac{(\gamma_0^2 - 1)^{1/4}}{G(\gamma_0)}\bar{u}_n(\bar{t}), \end{cases} \tag{8}$$

where $\bar{u}_n = u_n/c$ is the normalized momentum u_n with respect to the speed of light c, and $\bar{t} = \frac{t}{T_{RCL}}$. As an example,

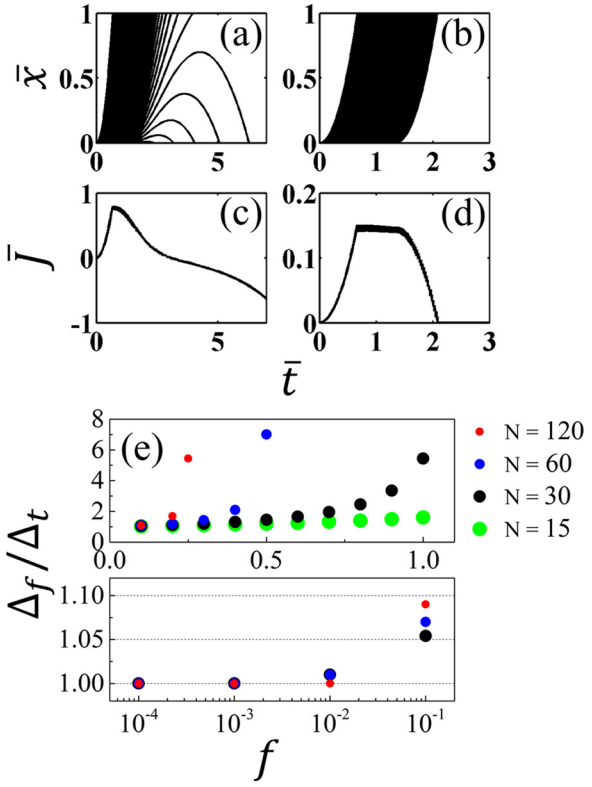

FIG. 3. The trajectories of each beam [(a) and (b)] and current densities [(c) and (d)] in a diode with gap spacing $d = 1.5$ mm and gap voltage $V_g = 30$ kV for $N = 60$ and $\Delta_t = 1$ps at $\sigma = 0.6\sigma_{N=30}$ [(a) and (c)] and $\sigma = 0.1\sigma_{N=30}$ [(b) and (d)]. (e) The dependence of Δ_f as a function of f for $\Delta_t = 1$ps for different N. The bottom subplot in Fig. 3(e) is a magnification of top subplots in the range of very small $f = 0.0001$–0.1.

we use $d = 1.5$ mm and $\Delta_t = 100$ fs, but at higher gap voltage $V_g = 5.11$ MV (10 times higher than 511 kV) to verify whether the convergence at $f = 0.1$ remains valid. In Fig. 4, each of the time intervals Δ_i (the time interval between ith beam to $(i+1)$th beam) is plotted with different factors $f = 0.1$, 0.5, and 1. For comparison, the classical cases (30 kV) are plotted in symbols for comparison. Here, we have $N_{max} \cong \left\lceil \frac{T_0}{\Delta_t} \right\rceil = 23$. Examination of this figure clearly shows that there is also zero pulse distortion $\Delta_i \backsimeq \Delta_t$ at $f = 0.1$ for the relativistic case. In fact, the relativistic case [5.11 MV] has even smaller distortion as compared to the classical case [30 kV], especially at a large $f = 0.5$ and $= 1$.

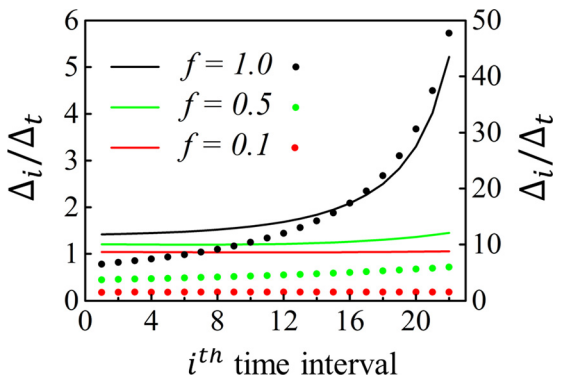

FIG. 4. The normalized calculated time intervals Δ_i/Δ_t for different $f = 0.1$, 0.5, and 1 in the relativistic regime of $V_g = 5.11$ MV (solid lines, plotted on the left y-axis) and in the classical regime of $V_g = 30$ kV (symbols, plotted on the right y-axis).

Here, we point out that the assumption of using $\Delta_x \cong \frac{1}{2}\left(\frac{qE_0}{m}\right)\Delta_t^2$ may be one of the reasons for the differences between the theory and the numerical calculations. It is difficult to obtain simple analytical expression to describe the dynamics of each charge sheet including space charge effects, thus we have assumed uniform spatial sheet separations to give a rough value, which can be adjusted later through f by numerical calculations. Another approximation that can be used is $\Delta_x = d/N_{max}$, where $N_{max} \cong \frac{T_0}{\Delta_t}$, and $T_0 \cong \sqrt{2d/\left(\frac{qE_0}{m}\right)}$ is the transit time of a single charge sheet. However, this also requires some tuning in comparison with exact numerical solution. As an example ($d = 1.5$ mm, $V_g = 30$ kV, and $\Delta_t = 100$ fs), we have $N_{max} = 30$, $\Delta_x \cong \frac{1}{2}\left(\frac{qE_0}{m}\right)\Delta_t^2 = 26\,\mu$m, and $\Delta_x = d/N_{max} = 57\,\mu$m, which gives $\frac{\sigma_{30}}{\sigma_1} = 0.044$, and $\frac{\sigma_{30}}{\sigma_1} = 0.074$, respectively, [according to Eq. (3)]. This indicates that the $\Delta_x = d/N_{max}$ approximation suggests a higher charge density, which would require a smaller value of f in fitting to the numerical solution.

Finally, we comment on the validity of the charge sheet model. For typical 4D electron imaging systems,[5,23–27] the electron pulse length is within the range of $\tau_p \cong 1$ ps to 0.01ps. The corresponding range of the normalized pulse length is $X_{CL} \equiv \frac{\tau_p}{T_{CL}} \cong 10^{-2} \sim 10^{-6} \ll 1$, which is consistent with our model. Prior work by Valfells[12] and Zhang[17] has also clearly indicated that results based on the charge sheet model agree very well with particle-in-cell (PIC) or many-body simulation results, as long as $X_{CL} < 0.1$. In practical cases, the transverse effect should be considered. Typically, 1D approximation can be used only when the transverse size is much larger than the longitudinal size. However, it can be imaged that if the transverse effect is considered, the transverse electric force causes transverse pulse expansion and a decrease of the charge density. Therefore, the transverse effect may cause the time structure to be better than for the 1D case. This is expected to be verified by 3D PIC simulation in our future work.

In summary, we constructed a model to study the space charge effects of N number of short electron pulses injected into a diode with an applied voltage of up to a few MeV (including relativistic effects). Based on this model, we obtained a formula [Eq. (3)] that is able to determine the upper limit of the charge density per pulse to avoid distortion in the time interval between pulses. The critical value turns out to be about 10% of a constant that can be calculated by using Eq. (3), over a wide range of parameters. The model may be useful in the design of multiple-pulse electron beams for time resolved electron microscopy or free electron lasers.

The work was supported by the National Science Council under the Grant No. MOST 103-2112-M-008-004. Y. L. Liu and S. H. Chen would like to thank the National Center for High-Performance Computing for providing resources under the national project, "Taiwan Knowledge Innovation National Grid," and the support provided by the National Center for Theoretical Sciences, Taiwan, ROC. Y. L. Liu was supported by the Singapore MOE T2 Grant

(T2MOE1401) as a research staff member at SUTD. P.Z. was supported by AFOSR Grant No. FA9550-14-1-0309.

[1]E. Brüche, Z. Phys. **86**, 448 (1933).
[2]D. Bayer, C. Wiemann, O. Gaier, M. Bauer, and M. Aeschlimann, J. Nanomater. **2008**, 249514.
[3]H. Spiecker, O. Schmidt, C. Ziethen, D. Menke, U. Kleineberg, R. C. Ahuja, M. Merkel, U. Heinzmann, and G. Schönhense, Nucl. Instrum. Methods Phys. Res., Sect. A **406**, 499 (1998).
[4]G. H. Fecher, O. Schmidt, Y. Hwu, and G. Schönhense, J. Electron. Spectrosc. Relat. Phenom. **126**, 77 (2002).
[5]A. H. Zewail and J. M. Thomas, *4D Electron Microscopy: Imaging in Space and Time*, 1st ed. (Imperial College Press, London, Hackensack, NJ, 2009).
[6]E. Bauer, J. Electron. Spectrosc. Relat. Phenom. **185**, 314 (2012).
[7]C. D. Child, Phys. Rev. (Series I) **32**, 492 (1911).
[8]I. Langmuir, Phys. Rev. **21**, 419 (1913).
[9]J. W. Luginsland, Y. Y. Lau, and R. M. Gilgenbach, Phys. Rev. Lett. **77**, 4668 (1996).
[10]Y. Y. Lau, Phys. Rev. Lett. **87**, 278301 (2001).
[11]W. S. Koh, L. K. Ang, and T. J. T. Kwan, Phys. Plasmas (1994-Present) **12**, 053107 (2005).
[12]Á. Valfells, D. W. Feldman, M. Virgo, P. G. O'Shea, and Y. Y. Lau, Phys. Plasmas (1994-Present) **9**, 2377 (2002).
[13]W. S. Koh, L. K. Ang, and T. J. T. Kwan, Phys. Plasmas (1994-Present) **13**, 063102 (2006).
[14]L. K. Ang and P. Zhang, Phys. Rev. Lett. **98**, 164802 (2007).
[15]L. Ang, T. Kwan, and Y. Lau, Phys. Rev. Lett. **91**, 208303 (2003).
[16]Y. B. Zhu, P. Zhang, A. Valfells, L. Ang, and Y. Lau, Phys. Rev. Lett. **110**, 265007 (2013).
[17]P. Zhang, W. S. Koh, L. K. Ang, and S. H. Chen, Phys. Plasmas (1994-Present) **15**, 063105 (2008).
[18]C. K. Birdsall and W. B. Bridges, *Electron Dynamics of Diode Regions* (Academic, New York, 1966).
[19]W. B. Bridges, J. I. Frey, and C. K. Birdsall, IEEE Trans. Electron Devices **12**, 264 (1965).
[20]Y. L. Liu, S. H. Chen, W. S. Koh, and L. K. Ang, Phys. Plasmas (1994-Present) **21**, 043101 (2014).
[21]M. R. Freeman and W. K. Hiebert, *Spin Dynamics in Confined Magnetic Structures I* (Springer, 2002), p. 93.
[22]S. Woutersen, U. Emmerichs, and H. J. Bakker, Science **278**, 658 (1997).
[23]J. S. Baskin, H. Liu, and A. H. Zewail, Proc. Natl. Acad. Sci. U.S.A. **111**, 10479 (2014).
[24]P. Baum and A. H. Zewail, Proc. Natl. Acad. Sci. U.S.A. **104**, 18409 (2007).
[25]O.-H. Kwon and A. H. Zewail, Science **328**, 1668 (2010).
[26]H. S. Park, J. S. Baskin, and A. H. Zewail, Nano Lett. **10**, 3796 (2010).
[27]A. H. Zewail, Annu. Rev. Phys. Chem. **57**, 65 (2006).
[28]A. H. Zewail, Science **328**, 187 (2010).
[29]R. K. Li and P. Musumeci, Phys. Rev. Appl. **2**, 024003 (2014).
[30]Y. Zhu and L. K. Ang, Appl. Phys. Lett. **98**, 051502 (2011).
[31]B. J. Siwick, J. R. Dwyer, R. E. Jordan, and R. J. D. Miller, J. Appl. Phys. **92**, 1643 (2002).